Journal of Physics and Chemistry of Solids 95 (2016) 106–113

Contents lists available at ScienceDirect

Journal of Physics and Chemistry of Solids

journal homepage: www.elsevier.com/locate/jpcs

Effect of point defects on the properties of silicene-like BSi_3 sheets from first-principles

Seifollah Jalili [a,b,*], Mojdeh Akhavan [b], Jeremy Schofield [c]

[a] Department of Chemistry, K. N. Toosi University of Technology, P. O. Box 15875-4416, Tehran, Iran
[b] Computational Physical Sciences Research Laboratory, School of Nano-Science, Institute for Research in Fundamental Sciences (IPM), P.O. Box 19395-5531, Tehran, Iran
[c] Chemical Physics Theory Group, Department of Chemistry, University of Toronto, 80 Saint George Street, Toronto, Ontario, Canada, M5S 3H6

ARTICLE INFO

Article history:
Received 26 December 2015
Received in revised form
19 March 2016
Accepted 15 April 2016
Available online 19 April 2016

Keywords:
Hexagonal BSi_3
Monolayers
Defects
Reconstructions
Electronic structure

ABSTRACT

Density functional theory calculations are used to investigate the impact of point defects on BSi_3 nanosheets. It is shown that the defects have low formation energies and are likely to form in BSi_3 sheets. The divacancies with missing Si an B atoms are more probable than those which have two missing Si atoms and the diantisite $(BSi)_{anti}$ is also more probable than $(BB)_{anti}$. It is found that the structural reconstructions caused by bond rotation in divacancies continuously lower the formation energies. Interestingly, unlike graphene or many other sheets, the presence of point defects does not change the planar structure and metallic behavior of BSi_3 and all systems are nonmagnetic. The planar and metallic BSi_3 sheets can therefore be used in devices, without any concern about the presence of defects.

1. Introduction

Searching for new two-dimensional (2D) nanomaterials with novel mechanical, electronic, and magnetic properties has become an active field in nanotechnology since the first isolation of graphene in 2004 [1]. Among the various 2D materials, silicene [2], the silicon analog of graphene, has been the subject of many research efforts. Similar to graphene, silicene nanosheet has a honeycomb structure with single-atom thickness and a linear Dirac cone, resulting in an electric conductance which is comparable to that of graphene [3,4]. In addition, it has some unique properties such as high structural stability and flexibility and high phonon scattering ability which make it a promising material for use in future electronic devices [5]. However, unlike graphene, the silicene sheets are not flat and a low buckling of about 0.44 Å has been reported for silicene monolayers using both density functional theory (DFT) calculations [4] and experimental methods [6].

By introducing dopant atoms into silicene sheets, one can obtain SiX or XSi_3 heterosheets which have various structural and electronic properties [7]. Among them, boron/silicon heterosheets such as BSi_3 (or SiB^8) sheets are especially interesting because of the importance of *p*-type boron dopants on silicon industry.

BSi_3 sheets are predicted, but not-yet synthesized planar structures composed of hexasilabenzene (c-Si_6) rings separated by boron atoms [7]. Another structure suggested for BSi_3 is an alternate arrangement of zigzag Si-atom chains and Si-B chains [9]. Recent DFT calculations show that the former structure, with hexagonal geometry, is lower in energy than the later, rectangular one. The highly stable planar structure of aromatic BSi_3 sheets (unlike silicene) is believed to be a result of the π-*p* interaction between c-Si_6 and boron atoms [10]. An interesting property of BSi_3 is its metallic behavior, which is preserved in different forms such as tubes, sheets, and ribbons with various chiralities and sizes. It also withstands mechanical strain and chemical functionalization [10].

In this paper various kinds of point defects, such as Stone-Wales (SW) defects, and single and double vacancies and antisites in BSi_3 sheets have been studied using density function theory (DFT) calculations. Various possible reconstructions of vacancy defects [11] due to Jahn–Teller distortion or bond rotations have also been taken into account. To the best of our knowledge, the defected forms of BSi_3 sheets have not been studied before.

The formation of a certain level of defects in a crystal is a likely phenomenon during the growth process. Defects may also be introduced during the preparation and characterization of nanomaterials. Since defects are ubiquitous, it is important to study the stability of various possible defected structures as well as the impact of defects on the material properties of BSi_3 sheets. As we will show, the planar geometry and metallic behavior of BSi_3 is

* Corresponding author at: Department of Chemistry, K. N. Toosi University of Technology, P. O. Box 15875-4416, Tehran, Iran.
E-mail address: sjalili@kntu.ac.ir (S. Jalili).

http://dx.doi.org/10.1016/j.jpcs.2016.04.004
0022-3697/

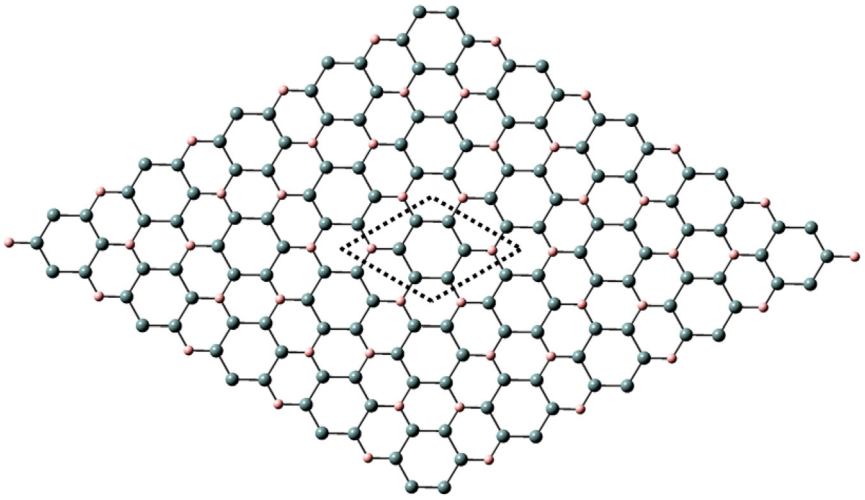

(a)

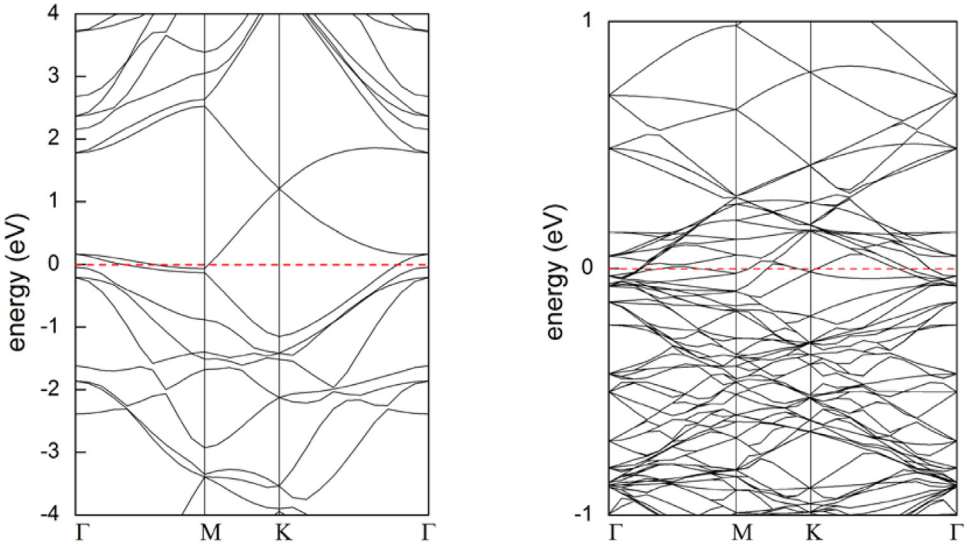

(b)

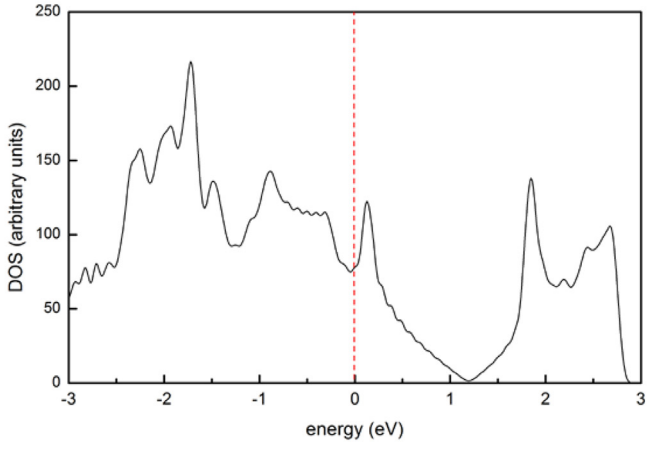

(c)

Fig. 1. (a) Structure of the pristine BSi_3 in a 5×5 supercell. The primitive unit cell is drawn by dashed lines. Si and B atoms are shown in gray and pink, respectively. (b) Electronic band structures for BSi_3 unit cell (left) and the 5×5 supercell (right). (c) Density of states plot for pristine BSi_3. The dotted lines in (b) and (c) indicate the position of the Fermi level. (For interpretation of the references to color in this figure legend, the reader is referred to the web version of this article.)

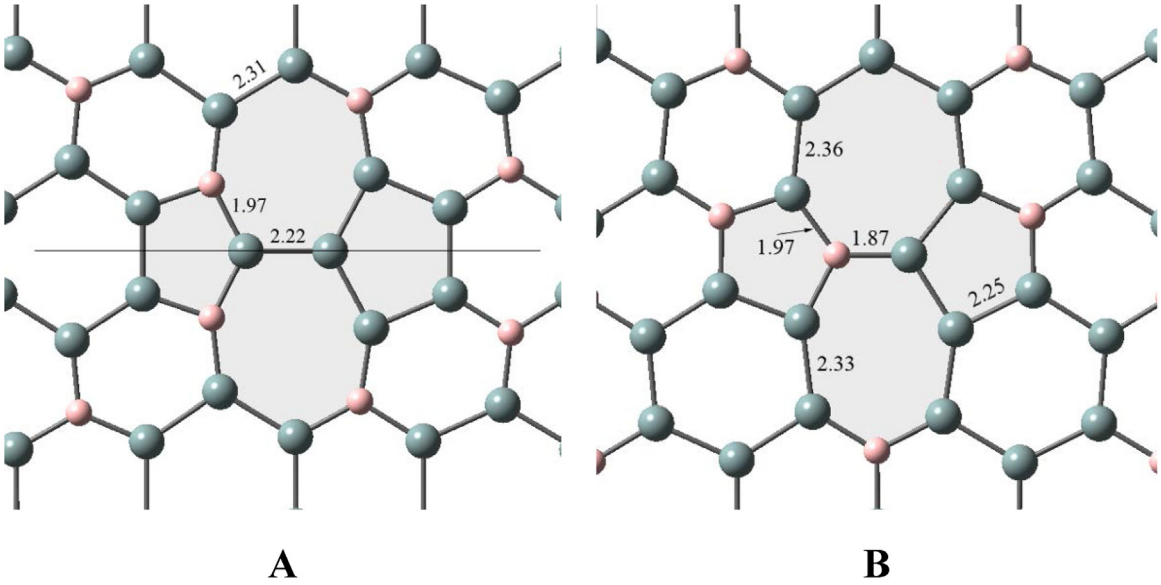

Fig. 2. Atomic structures of BSi3 sheets with SW defects generated from Si–Si (A) and Si–B (B) bond rotations.

preserved in all studied defected forms. On the other hand, BSi_3 sheets have been previously shown [12] to be good candidates for the anode material of lithium–ion batteries (LIBs) and the defects, which can be easily formed due to their low formation energies, may enhance the Li adsorption and diffusion properties of BSi_3 sheets for use in lithium-ion batteries.

2. Methods

DFT calculations were performed using the plane wave pseudopotential technique implemented in the QUANTUM ESPRESSO package [13]. The generalized gradient approximation (GGA) with the Perdew–Burke–Ernzerhof (PBE) functional [14] was used for the exchange-correlation interactions. The core electrons were described by the projected augmented wave (PAW) potential [15]. The plane wave cutoff energy was set to be 400 eV and the convergence criterion of 10^{-5} eV was used for the total energy.

The primitive cell of the hexagonal BSi_3 sheet is shown by dashed lines in Fig. 1(a). It contains six Si and two B atoms [10]. The positions of atoms and the lattice constant in BSi_3 unit cell were fully relaxed and used to construct a 5×5 supercell (shown in Fig. 1(a)) to avoid the interactions between defects and their periodic images. A vacuum space of 20 Å was used along the *z*-direction to simulate a 2D periodic system in the *xy* plane. The overall dimensions of the hexagonal supercell were $36.55 \times 36.55 \times 20$ Å^3.

Point defects from five main categories, namely Stone–Wales (SW), monovacancy, monoantisite, divacancy, and diantisite, were created in pristine BSi_3 sheets to obtain 26 structures, with the possible structures obtained from vacancy reconstructions included. The systems were fully relaxed using a force convergence threshold of 0.03 eV/Å. The Brillouin zone sampling was performed using a $2 \times 2 \times 1$ Monkhorst-Pack [16] *k*-point mesh including the Γ point. For the calculation of energies, the *k*-point mesh was increased to $8 \times 8 \times 1$. Because of the possibility of magnetization, spin-polarization was taken into account in all calculations.

The binding energy (E_b) of the pristine BSi_3 sheet was defined as $E_b = [E(B) + 3E(Si) - E(BSi_3)]/4$, where the energy terms are the total energies of the boron atom, silicon atom, and the BSi_3 unit, respectively. The total energies of isolated (B or Si) atoms were calculated using a cubic cell length of 40 Å.

3. Results and discussion

As a first step, the computational method was validated against experimental and computational data for the BSi_3 unit cell. The Si–Si and Si–B bond lengths in the optimized BSi_3 unit cell were found to be 2.29 and 1.94 Å and the unit cell parameter was 7.31 Å, in agreement with previous DFT calculations [7,10]. The binding energy for the unit cell was calculated to be 4.36 eV/atom, which is same as the binding energy of the pristine 5×5 BSi_3 supercell. In comparison, Tan et al. [10] obtained a value of 4.10 eV/atom and the binding energy reported by Ding and Wang [7] was 4.27 eV/atom. There is also an experimental value of 4.62 eV/atom for the cohesive energy of the diamond cubic silicon [8], which is near the value of 4.60 eV/atom we obtained. These comparisons suggest that the methods utilized here are adequate for calculating the energetics and structural properties of BSi_3 sheets.

The band structures of BSi_3 unit cell and supercell along the high symmetry path of ΓMKΓ are shown in Fig. 1(b). As reported before [10], pristine BSi_3 is a metal, with bands crossing the Fermi level at the M point. In the supercell however, the bands cross the Fermi level at the K point instead, which is due to zone folding. Consistent with band structures, density of states (DOS) plot for the pristine BSi_3 in Fig. 1(c) shows a nonzero DOS value at Fermi energy, indicating metallic behavior. The Dirac cone feature of silicone [4] is preserved in BSi_3 and is located above the Fermi level. This shows that boron atoms increase the conductivity of silicene by a *p*-type doping effect. Our calculations show that all of the defected monolayers are also metallic and their DOS plots are very similar to that of pristine BSi_3 sheet, so they have been omitted to avoid redundancy.

During the geometry optimization, some of the structures relaxed to others, leaving 16 distinct structures out of 26 initially chosen geometries. Figs. 2–5 show the optimized BSi_3 sheets with various types of defects. In these figures we have indicated all the distances which deviate more than (or equal to) 0.03 Å from the corresponding values in the pristine sheet and the straight lines denote an axis or plane of symmetry. All systems are planar and stable, without any evidence of meta-stable structures appearing during the optimization process, a behavior which is similar to the

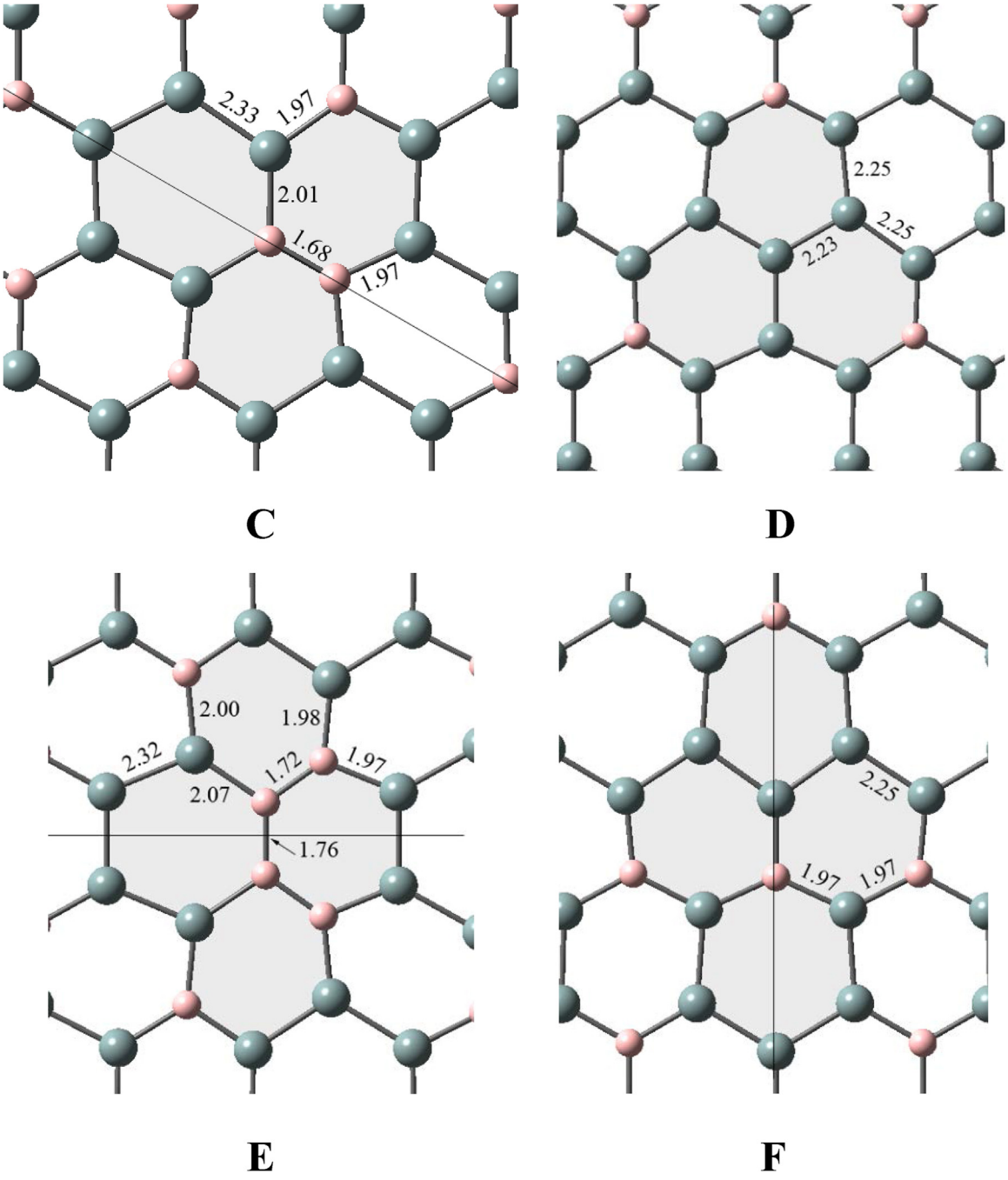

Fig. 3. Optimized structures for BSi_3 sheets with antisite defects. Refer to Table 1 for labeling.

case of defected BC_3 sheets [17]. However unlike the case of BC_3 sheets, defects do not modify the electronic and magnetic properties of BSi_3 sheets and all of the defected BSi_3 sheets remain metallic and non-magnetic, and therefore have the same properties as the pristine sheet, as noted in the discussion about band structures.

The stability of defected structures can be examined using defect formation energies. For the SW defects, formation energy (E_f) was calculated from the total energy difference between the defected and perfect BSi_3 sheets. For monoantisites (atom of X in place of Y):

$$E_f(\text{antisite}) = E_{\text{defected}} - E_{\text{perfect}} - \mu[X] + \mu[Y] \quad (1)$$

and for monovacancies (missing X atom)

$$E_f(\text{vacancy}) = E_{\text{defected}} - E_{\text{perfect}} + \mu[X] \quad (2)$$

Here E_{defected} and E_{perfect} are the total energies of defected and perfect systems, respectively and the μ's are the chemical potentials (energy per atom) for the boron or silicon atoms. The chemical potentials are generally regarded as variables that change to reflect different experimental conditions, subject to the thermodynamic equilibrium constraint:

$$\mu[\text{B}] + 3\mu[\text{Si}] = \mu\left[\text{BSi}_3\right] \quad (3)$$

where $\mu[BSi_3]$ is the chemical potential (or energy per formula unit) of the BSi_3 sheet.

The equilibrium condition in Eq. (3) allows μ values to only change within specific ranges. Two extreme conditions can be defined: At B-rich conditions, μ[B] is computed as the energy per

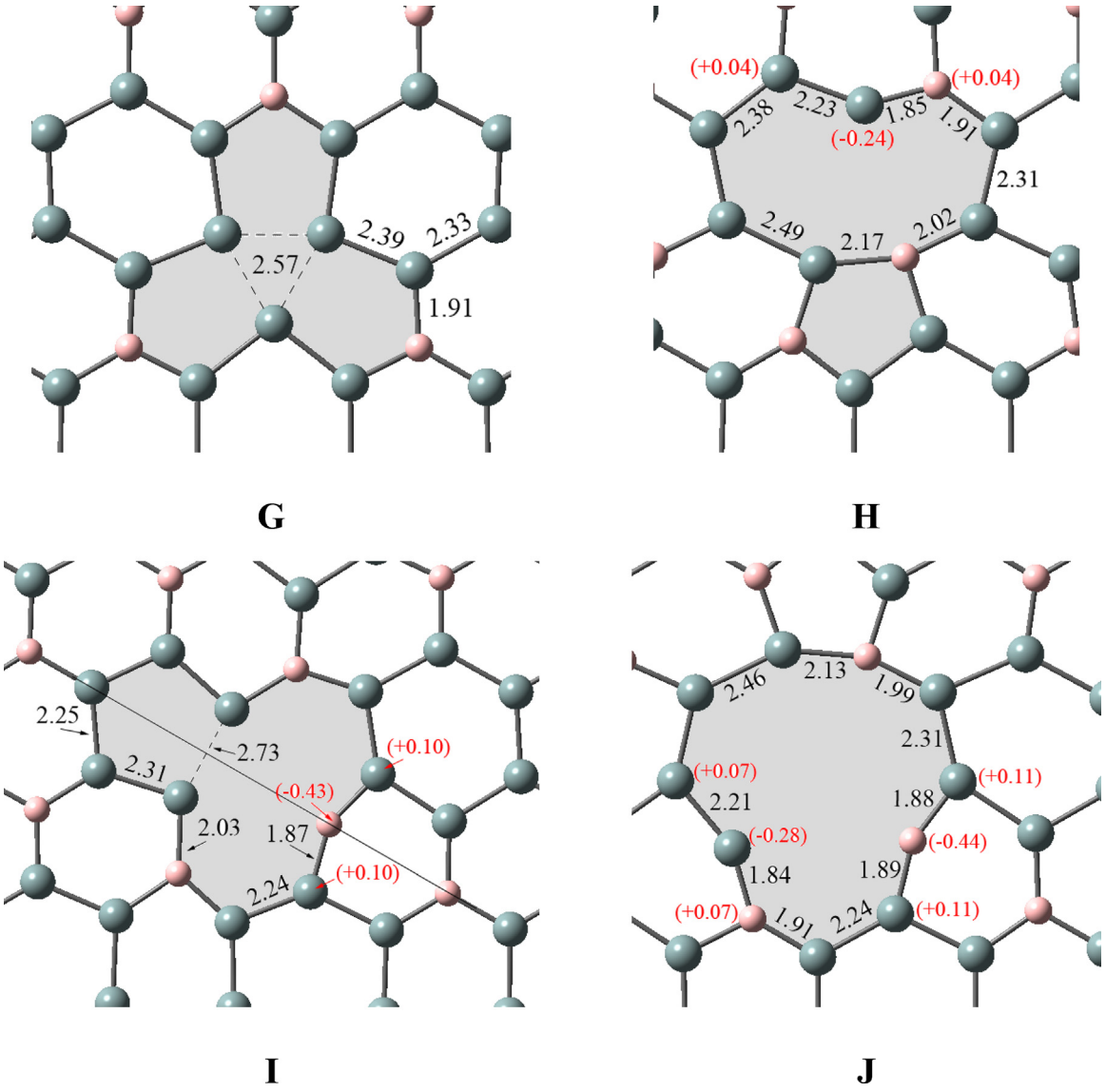

Fig. 4. Optimized geometries of boron **(G)** and silicon (**H** and **I**) monovacancies and the non-reconstructed divacancy V_{SiSi} **(J)** in the BSi_3 sheet. The positive (negative) values in parentheses show the amount of charge gained (lost) by atoms.

atom in the crystal structure of rhombohedral α-boron [18] and μ [Si] is obtained from Eq. (3). Alternatively at Si-rich conditions, μ [Si] is defined as the energy per atom in diamond (cubic) silicon and μ[B] is given by Eq. (3). Table 1 shows the E_f values for defected sheets for B-rich and Si-rich conditions. Based on the above definitions, a smaller (positive) value of E_f indicates that the defect can be more easily induced by irradiation or other processes.

The calculation of chemical potential was performed for one unit cell of diamond silicon (with 2 atoms) or α-boron (having 12 atoms) using a $8\times8\times8$ grid of k-points. For divacancies and diantisites, the μ terms are multiplied by the number of removed or added atoms.

The formation energies of defects in BSi_3 sheets are systematically lower than the defect formation energies in silicone [19] (2.09–3.77 eV) and grapheme [11] (4.5–8.7 eV). As shown in Table 1, the monoantisite Si_{anti} (**D**) has negative formation energy in B-rich surroundings, whereas the formation energies of boron mono- and diantisite defects (**C** and **E**) are negative in Si-rich conditions. The negative formation energies imply that these types of effects are more likely formed in BSi_3 sheets. It should be noted that the E_f values have been obtained at 0 K and the room temperature effects have not taken into account. Negative formation energies for antisite defects have been also obtained in the study of defected BC_3 sheets [17], but the trend of values is opposite to our case, i.e. C_{anti} has a negative E_f in the C-rich surroundings and vice versa.

In Fig. 2, two types of Stone–Wales defects in BSi_3 sheet are shown. These defects are formed by an in-plane rotation of a Si–Si (**A**) or Si–B (**B**) bond by 90°. At a result, a system of two pentagons and two heptagons (55–77) are formed. Compared to the pristine BSi_3 sheet, the rotated bond in the optimized geometry has been shortened by 0.06 or 0.07 Å, while the neighboring Si–B bonds are 0.03 Å longer in both structures. The Si–Si and Si–B bond rotations reduce the symmetry to C_{2v} and C_s, respectively. The **B** system undergoes greater structural modifications relative to the pristine sheet than **A**, especially in Si–Si bond lengths, but it has lower formation energy.

The optimized structures of BSi_3 sheets with mono- and diantisite defects are shown in Fig. 3. In the monoantisite B_{anti} (**C**), one carbon atom in BSi_3 is replaced by boron, and it can be formed by the adsorption of a B atom at a Si vacancy site. As a result, two Si–Si bonds are removed, while one additional Si–B and one B–B bond are formed. The length of the new homogeneous B–B bond is 1.68 Å, which is close to the value (1.71 Å) reported [17] for a BC_3

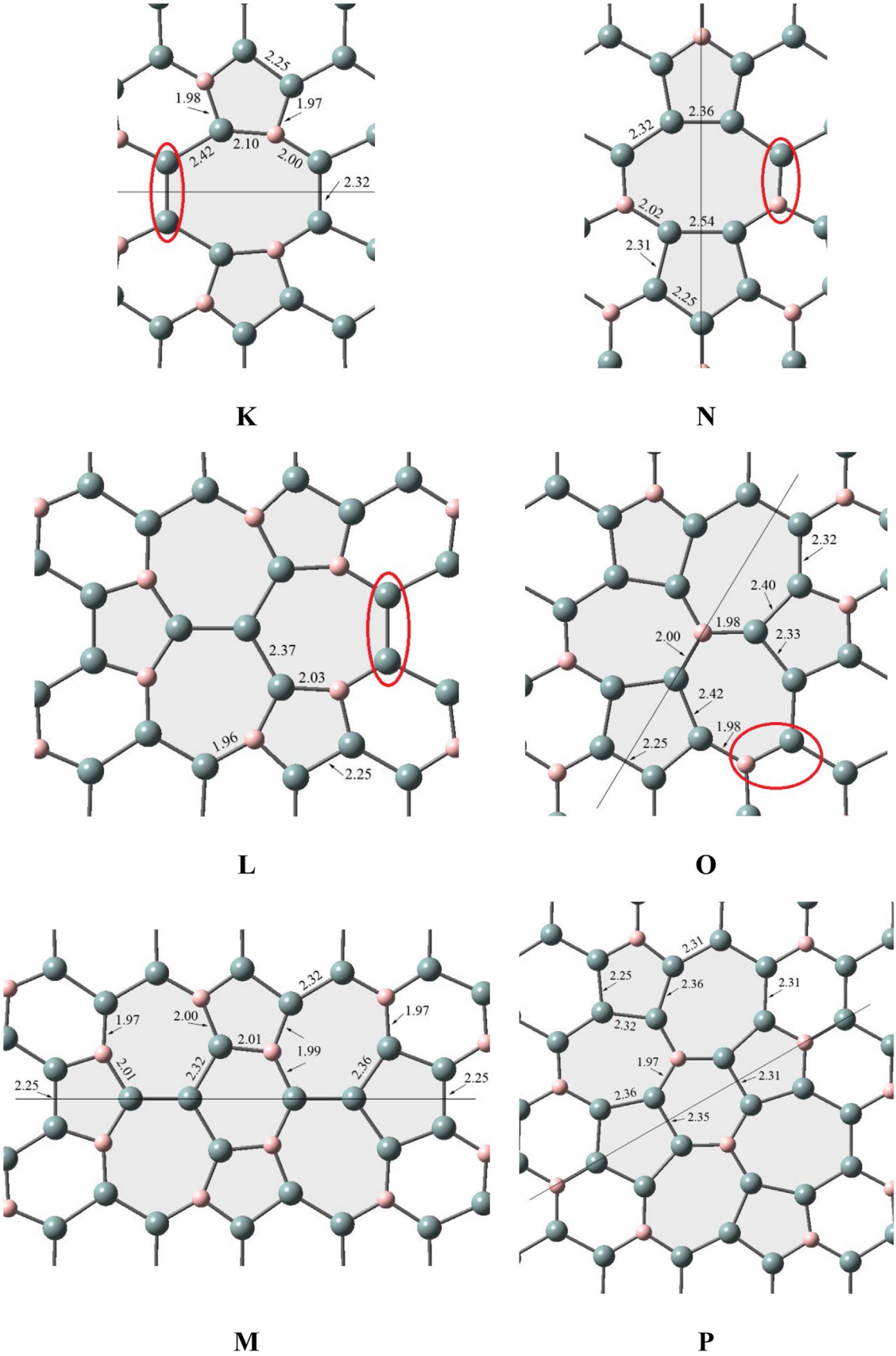

Fig. 5. Atomic Structures of reconstructed divacancy defects V_{SiSi} and V_{SiB} in the BSi_3 sheet. Refer to Table 1 for labeling.

Table 1
Defect formation energies (E_f, eV) for defected BSi_3 sheets. For vacancy and antisite defects, separate values of E_f are given for B-rich and Si-rich conditions.

System	Label	E_f		System	Label	E_f	
		B-rich	Si-rich			B-rich	Si-rich
SW-SiSi	**A**	1.62		V_{Si}-2	**I**	3.59	2.67
SW-SiB	**B**	1.57		V_{SiSi}	**J**	5.22	3.39
B_{anti}	**C**	1.74	−1.92	V_{SiSi}-(5-8-5)	**K**	4.09	2.26
Si_{anti}	**D**	−1.03	2.64	V_{SiSi}-(555-777)	**L**	2.99	1.15
$(BB)_{anti}$	**E**	4.12	−3.21	V_{SiSi}-(5555-6-7777)	**M**	2.73	0.89
$(BSi)_{anti}$	**F**	0.18	0.18	V_{SiB}-(5-8-5)	**N**	1.99	3.83
V_B	**G**	1.29	4.04	V_{SiB}-(555-777)	**O**	0.99	2.82
V_{Si}-1	**H**	3.49	2.58	V_{SiB}-(5555-6-7777)	**P**	0.72	2.55

sheet with a B_{anti} defect. As shown in Fig. 3, the Si–B bonds near the B–B bond in structure **C** are lengthened and the system has C_{2v} symmetry.

Another possible monoantisite in BSi_3 is Si_{anti} (**D**), which is the most symmetric (D_{3h}) among the antisite defects shown in Fig. 3. In this structure, three Si–B bonds are replaced by Si–Si bonds. It contains three equivalent hexagons and shows a slight deviation in Si–Si bond lengths relative to the pristine sheet.

In the diantisite $(BB)_{anti}$ structure (labeled **E** in Fig. 3), two neighboring Si atoms are replaced by B atoms. As a result, three Si–Si bonds are removed and three B–B bonds are formed. Similar to the case in the BC_3 sheet [17], the central B–B bond has a larger bond length than the other two B–B bonds. For the diantsite $(BSi)_{anti}$ defect (labeled **F** in Fig. 3), the number of bonds does not change. Like $(BB)_{anti}$, the symmetry of $(BSi)_{anti}$ is C_{2v}, but the formation energy is much lower.

Vacancies are closely related to antisites and are formed by missing atom(s) in crystals. The mono- and divacancies in BSi_3 sheets are shown in Figs. 4 and 5. When one atom is removed in a monovacancy, three under-coordinated atoms (or dangling bonds) are introduced around the vacancy position. Under certain circumstances, the system can undergo a Jahn-Teller distortion which leads to the saturation of dangling bonds and formation of new bonds. For this reason, various structures such as (5–9) and (55–66) reconstructions [20] have been considered in the optimization of monovacancy systems in addition to the so-called "native" vacancy defects. The structures **G**, **H**, and **I** in Fig. 4 are the stable monovacancies obtained in BSi_3. Other geometries relax to these structures during the structural optimization.

In the BSi_3 sheet with a single B vacancy defect, V_B, the most stable form (**G**) has three under-coordinated atoms that are symmetrically arranged around the position of the missing B atom. The formation energy of **G** is relatively low (in B-rich conditions) and the distances between (non-bonded) Si atoms in the resulting triangle are 2.57 Å, which are 0.78 Å shorter than those in pristine BSi_3 sheet. The Si–Si bonds next to the central Si atoms are elongated to 2.39 Å, but the next Si–B bonds are slightly shorter than those in the defect-free BSi_3 sheet. It is clear that although the atoms move through each other, no Jahn–Teller distortion occurs. This is due to the large atomic radius of Si atoms. The D_{3h} symmetry is maintained. A similar symmetric structure has been observed for V_B in BC_3 sheets [17].

For single Si vacancy defect, V_{Si}, two stable structures have been obtained, namely, V_{Si}-1 (**H**) and V_{Si}-2 (**I**). As shown in Fig. 4, a new Si–B bond is formed in structure **H** due to Jahn–Teller distortion, resulting in a (5–9) system. The two atoms are displaced in the optimized structure from an initial distance of 3.66 Å to the bonded distance of 2.17 Å. The formation energy of structure **H** is lower than that of **I** in which the two Si atoms approach each other from the initial distance of 3.96 Å, but don't form a bond. Structure **I** has C_{2v} symmetry and most of its bonds have been changed compared to the pristine structure.

In Fig. 4, a V_{SiSi} divacancy which is formed by removing two neighboring Si atoms is shown. A pentagon with a Si–B bond length of 2.13 Å and an 11-membered ring form, but the formation energy of this defect is high (specially in B-rich surroundings), and hence it is unlikely to form in BSi_3 sheets.

An interesting property of the systems shown in Fig. 4 is that although they all have one or more under-coordinated atoms, no magnetic moment is observed in any of the structures. The electrons prefer to delocalize in π bonding, which is probably due to structural distortions and/or charge transfer to neighboring atoms. Charge data in Fig. 4 shows that under-coordinated atoms lose electrons to their neighboring atoms and the amount of charge transfer for B is larger to that of Si. Non-magnetic monovacancy defects have also been obtained for V_C in SiC monolayers [21], as well as in BC_3 sheets [17] and nanotubes [22].

Divacancies can undergo structural reconstructions in a way leading to structures with two pentagons and one octagon (5–8–5) instead of the four hexagons that appear in perfect BSi_3. In the top row of Fig. 5, the (5–8–5) reconstructed rings for divacancies V_{SiSi} (**K**) and V_{SiB} (**N**) are depicted. However, there are other possible ways for them to lower their energy, i.e. one of the bonds may rotate by 90° (similar to SW defects) to form three pentagons and three heptagons (555–777), which in turn forms a (5555–6–7777) system by another bond rotation. The structures in Fig. 5 are the most stable forms among the various probabilities for bond rotation. The rotating bond is indicated by a red ellipse in structures **K**, **L**, **N**, and **O** in Fig. 5. All structures have C_{2v} symmetry, except **L** which has a D_{3h} point group.

As is evident from the data in Table 1, in B-rich conditions V_{SiB} is generally more favorable than V_{SiSi} and $(BSi)_{anti}$ is more favorable than $(BB)_{anti}$. Similar trend has been obtained for BC_3 sheets in a C-rich environment, where the formation energies of V_{BC} and $(BC)_{anti}$ are lower than those of V_{CC} and $(BB)_{anti}$, respectively [17]. The difference between formation energies of (5–8–5) and (555–777) systems is about 1 eV for both types of divacancies, which is similar to graphene [11], but unlike graphene, each reconstruction reduces the formation energy, so the final structures **M** and **P** have lowest formation erergies.

4. Conclusions

The effect of various kinds of point defects on the structure and electronic properties of a BSi_3 monolayer has been studied. The formation energies of defects are relatively low, suggesting that it is relatively easy to create point defects in BSi_3 sheets with only small structural distortions. The formation energy per missing atom in divacancies is much lower than that for a monovacancy, which suggests they are thermodynamically more favorable than monovacancies.

Our computations reveal that like the pristine sheet, all defected systems are metallic, planar, and non-magnetic. The large size of Si atoms and charge transfer interactions do not allow magnetic moments to be developed in defected structures with under-coordinated atoms. These results suggest that the interesting properties of BSi_3 sheets are maintained upon defect formation, in addition to other structural changes which have been studied before [10]. This behavior is probably useful in the practical application of BSi_3 sheets in nanotechnology. The defects may also improve the metal binding ability of BSi_3 sheets, which suggests they may be suitable for many potential applications, such as in lithium-ion batteries.

Acknowledgment

This work has been supported (project number 93051016) by Iran National Science Foundation (INSF). Calculations were performed using WestGrid (www.westgrid.ca) and Compute Canada Calcul Canada (www.computecanada.ca) computing facilities.

References

[1] K.S. Novoselov, A.K. Geim, S.V. Morozov, D. Jiang, Y. Zhang, S.V. Dubonos, I. V. Grigorieva, A.A. Firsov, Science 306 (2004) 666.
[2] D. Jose, A. Datta, Acc. Chem. Res. 47 (2014) 593.
[3] G.G. Guzmán-Verri, L.C. Lew Yan Voon, Phys. Rev. B 76 (2007) 075131.
[4] S. Cahangirov, M. Topsakal, E. Aktürk, H. Şahin, S. Ciraci, Phys. Rev. Lett. 102 (2009) 236804.
[5] N.J. Roome, J.D. Carey, ACS Appl. Mater. Interfaces 6 (2014) 7743.
[6] B. Lalmi, H. Oughaddou, H. Enriquez, A. Kara, S. Vizzini, B. Ealet, B. Aufray, Appl. Phys. Lett. 97 (2010) 223109.
[7] Y. Ding, Y. Wang, J. Phys. Chem. C 117 (2013) 18266.
[8] A. Hansson, F. de Brito Mota, R. Rivelino, Phys. Rev. B 86 (2012) 195416.
[9] J. Dai, Y. Zhao, X. Wu, J. Yang, X.C. Zeng, J. Phys. Chem. Lett. 4 (2013) 561.
[10] X. Tan, F. Li, Z. Chen, J. Phys. Chem. C 118 (2014) 25825.
[11] F. Banhart, J. Kotakoski, A.V. Krasheninnikov, ACS Nano **5** (2011) 26.
[12] X. Tan, C.R. Cabrera, Z. Chen, J. Phys. Chem. C 118 (2014) 25836.
[13] P. Giannozzi, et al., J. Phys.: Condens. Matter 21 (2009) 395502.
[14] J.P. Perdew, K. Burke, M. Ernzerhof, Phys. Rev. Lett. 77 (1996) 3865.
[15] P.E. Blöchl, Phys. Rev. B 50 (1994) 17953.
[16] H.J. Monkhorst, J.D. Pack, Phys. Rev. B 13 (1976) 5188.
[17] Y. Ding, Y. Wang, J. Ni, J. Phys. Chem. C 114 (2010) 12416.
[18] A.R. Oganov, J. Chen, C. Gatti, Y. Ma, Y. Ma, C.W. Glass, Z. Liu, T. Yu, O. O. Kurakevych, V.L. Solozhenko, Nature 457 (2009) 863.
[19] J. Gao, J. Zhang, H. Liu, Q. Zhang, J. Zhao, Nanoscale 5 (2013) 9785.
[20] S. Berber, A. Oshiyama, Physica B 376–377 (2006) 272.
[21] X. He, T. He, Z. Wang, M. Zhao, Physica E 42 (2010) 2451.
[22] S. Jalili, M. Akhavan, J. Schofield, J. Phys. Chem. C 116 (2012) 13225.